Characterisation of cobalt–zinc hydroxycarbonates and their products of decomposition

Thomas Baird,[a] Kenneth C. Campbell,[a] Peter J. Holliman,[a] Robert W. Hoyle,[a] Diane Stirling,*[a] B. Peter Williams[b] and Michael Morris[c]

[a]*Chemistry Department, University of Glasgow, Glasgow, UK G12 8QQ*
[b]*ICI Katalco, P O Box 1, Billingham, Cleveland, UK TS23 1LB*
[c]*University College Cork, Ireland*

A series of cobalt–zinc hydroxycarbonate precursors with nominal Co/Zn atomic ratios of 0/100, 10/90, 20/80, 30/70, 40/60, 50/50, 70/30, 90/10 and 100/0 have been synthesized from their mixed metal nitrates and ammonium carbonate by a coprecipitation route. X-Ray and electron diffraction studies of the precursors revealed that hydrozincite, $Zn_5(CO_3)_2(OH)_6$, was the major phase at Co/Zn ratios $\leqslant$ 30/70 and spherocobaltite, $CoCO_3$, predominated at Co/Zn ratios of 50/50 to 90/10. The Co/Zn 100/0 precursor formed only the metastable basic carbonate $Co(CO_3)_{0.5}(OH)_{1.0}\cdot 0.1H_2O$. UV–VIS–NIR diffuse reflectance spectroscopy revealed that the cobalt was present in the 2+ oxidation state in an octahedral environment in all the precursors. Decomposition of the Co/Zn precursors at 350 °C resulted in the formation of ZnO as the major phase at low Co loadings and Co_3O_4 as the major phase at high loadings. The highest surface areas were attained from the decomposition of basic cobalt carbonate or spherocobaltite containing little or no zinc in solid solution. XPS studies of the oxides revealed that only Co^{3+} and Zn^{2+} ions were present at the surface at Co/Zn ratios $\leqslant$ 30/70 indicating the presence of the 'surface spinel', $ZnCo_2O_4$. Co^{2+} was detected at higher Co loadings.

High surface area metal oxides have an important role in the removal of species such as H_2O, CO_2 and H_2S from feedstocks and refinery effluent which would otherwise contribute to acid rain.[1] More recently, modified ZnO[2] and mixed metal oxides[3,4] have been developed, some of which have improved adsorbent capabilities. The adsorbent characteristics of the mixed oxides are largely dependent on their surface area, which is in turn governed by the morphology and homogeneity of the precursor. Coprecipitation of mixed metal salts with an alkaline carbonate at low supersaturation and constant pH provides a route to single-phase mixed metal carbonates and hydroxycarbonates[5] which form interdispersed high surface area mixed oxides on calcination.[6] Precipitation occurs by a heterogeneous nucleation process involving deposition of the solute on impurity particles in the solvent. Particle growth then ensues *via* diffusion of solute to the particle, adsorption at the solid/liquid interfacial layer, surface diffusion and incorporation of solute material into the crystal lattice.[7] The normal growth processes may be complicated further by competing dissolution and agglomeration processes. The rates of nucleation and particle growth are affected by the pH and temperature at which the reaction is carried out. The effective precipitate surface area then changes with time during the ageing of the precipitate in the mother liquor. Agglomeration, recrystallisation and surface modifications occur during ageing. The final morphology and composition of the precipitates is determined by a combination of the rates of nucleation and particle growth, ageing conditions of the precipitate in the mother liquor and habit modifications resulting from ions present either in solution or in the solvent.

The preparation of ZnO and Co_3O_4 by decomposition of their basic carbonates formed by coprecipitation routes is already documented.[8,9] Precipitation was carried out by mixing the metal nitrates with $NaHCO_3$ whilst maintaining the pH at 8. Hydrozincite, $Zn_5(CO_3)_2(OH)_6$, was formed when using zinc nitrate, and a new basic cobalt carbonate, $Co(CO_3)_{0.5}(OH)_{1.0}\cdot 0.1H_2O$, was identified in the preparation from the cobalt salt. Preparation of the mixed metal precursors has received less attention. Petrov *et al.*[10] used a sequential precipitation method in which the alkali was added to the zinc and cobalt nitrate salts so that the salts were precipitated out sequentially with rising pH, but this resulted in the formation of a basic cobalt–zinc hydroxynitrate species, $Zn_{1.66}Co_{3.34}(OH)_{8.82}(NO_3)_{1.26}(H_2O)_{2.23}$. Formation of the basic nitrate is undesirable since toxic nitrogen oxides are evolved on decomposition to the oxides. Klissurski and Uzanova[11] synthesised a high surface area zinc cobaltite from a Co–Zn hydroxycarbonate prepared at pH 9 by addition of zinc and cobalt nitrates to sodium carbonate, but the precursor phase was not examined in detail.

This paper describes studies carried out in our laboratory on the preparation and full characterisation of a series of cobalt–zinc hydroxycarbonates with nominal Co/Zn atomic ratios of 0/100, 10/90, 20/80, 30/70, 40/60, 50/50, 70/30, 90/10 and 100/0 and their products of decomposition. These oxides were prepared for use as absorbents for low-temperature gas desulfurisation, and their absorption behaviour will be reported in a subsequent paper.

Experimental

Precursor and oxide preparation and analysis

Precursors with nominal atomic ratios of Co/Zn 0/100, 10/90, 20/80, 30/70, 40/60, 50/50, 70/30, 90/10 and 100/0 were prepared by coprecipitation at low supersaturation and a constant pH of 7. Solutions of cobalt and zinc nitrates (1 mol dm^{-3}) in the appropriate ratios were pumped simultaneously with a 2 mol dm^{-3} ammonium carbonate solution into a mixing vessel at 70–75 °C. After addition of the solutions was completed (*ca.* 20 min), the precipitate was aged in the mother liquor for 30 min whilst being stirred vigorously. The solutions were then filtered and the solids washed with distilled water to remove any impurities. Finally the precursors were dried in an oven at 110 °C for 16 h. The precursors were ground finely in an agate mortar and calcined in air under static conditions in a muffle oven at 350 °C for 16 h.

The cobalt and zinc contents of all the precursors and oxides were determined by atomic absorption using a Perkin-Elmer 370A spectrometer. The metals were extracted by digestion in

concentrated nitric acid at *ca.* 50 °C. Diluted solutions of the extracted nitrates were then analysed quantitatively by comparison with standard solutions (BDH-Spectrosol). The precursors and oxides will be identified by their nominal loadings when referred to in the text of the paper. The coprecipitated precursors will be referred to as Co/Zn with a suffix indicating the nominal metal ratio. The suffix cal will be added for the calcined samples.

Precursor and oxide characterisation

X-Ray powder diffraction. The powder diffraction patterns were obtained using a Perkin-Elmer D60 diffractometer and Ni-filtered Co-Kα radiation ($\lambda = 1.7902$ Å). Scans were recorded between $2\theta = 12$ and 74° for the precursors, and $2\theta = 20$ to 100° for the oxides. In both cases the scan rate used was 2° min^{-1}.

Transmission electron microscopy. The samples were examined on either a JEOL 1200EX or a JEM-100C transmission electron microscope. Specimens were prepared by suspending them in water and then mounting them on carbon-filmed copper grids.

UV–VIS–NIR diffuse reflectance spectroscopy. Reflectance spectra were recorded, in the wavelength range 190–2500 nm, using a Perkin-Elmer Lambda 9 UV–VIS–NIR spectrometer equipped with a diffuse reflectance attachment. Barium sulfate, $BaSO_4$, was used as a standard.

IR spectroscopy. Spectra were obtained in transmission mode, between 4000 and 400 cm^{-1}, using a Phillips PU980 FTIR spectrometer.

Thermogravimetry. TG measurements were carried out using a Stanton Redcroft 1500 analyser. The ground samples (*ca.* 15 mg) were heated at 20 °C min^{-1} in air at a flow rate of 1 dm^3 h^{-1}. The calculated mass losses were determined to within ±2% and the temperatures of decomposition to ±5%.

Surface area determination. BET surface areas (N_2, 77 K) were calculated from five-point adsorption isotherms. The surface areas were obtained using either a Digisorb 2500 or a Flowsorb 2300 Micromeritics instrument. Samples were outgassed at 140 °C for 8 h before surface area measurements.

X-Ray photoelectron spectroscopy.

Qualitative analysis. X-Ray photoelectron spectra were obtained using Al-Kα ($h\nu = 1486.6$ eV) monochromated radiation with a Surface Science Instruments M-Probe Spectrometer connected to a Hewlett Packard Vectra RS/20C computer for data acquisition and analysis. The analysis chamber was evacuated to $< 1 \times 10^{-8}$ Torr before running the spectra. The spectra were recorded at room temperature and at low X-ray fluxes (anode operating at 10 kV and 22 mA). The data analysis procedure generally involved background subtraction by a Shirley-type integral profile and a curve-fitting procedure by a least-squares method.

The spectra were analysed in terms of the relative peak area intensities, the full-width at half-maximum height (FWHM) of the peaks, and the chemical shifts of the $2p_{3/2}$ transitions of zinc and cobalt, and the oxygen 1s transition. Spectra were collected with a pass energy of 50 eV. The experimental errors were estimated to be ±0.2 eV for the photoelectron peak binding energy positions.

The samples were loaded using double-sided Scotch tape. A low-energy electron-flood gun was used and residual charging effects were corrected for all the hydroxycarbonate precursors and oxides. Charge referencing can be a major problem in XPS studies of insulators. Charge referencing was carried out on the data collected before analysis.[12]

The precursors were charge referenced by the internal standard method to the carbonate C 1s, $E_B = 289.1$ eV. The O 1s peak associated with the carbonate group varies only from 531.0 to 531.2 eV which is within the experimental error. It is this lack of variation that allows the carbonate to be used confidently as it suggests that it is not affected to any great extent by the surrounding environment.

Adventitious carbon was not used to charge reference the oxides because the C 1s peak appeared outwith the parameters of the narrow energy scan selected for several of the samples due to large charge shifts. Charging was referenced to the O 1s peak at $E_B = 530.0$ eV. It is appreciated that the chemical environment within the series of oxides will vary and hence affect the true position of the O 1s peak.

Quantitative analysis. For Co and Zn present at the surface of a powder sample their relative atomic ratios can be calculated using

$$\frac{n_{Co}}{n_{Zn}} = \frac{I_{Co}}{I_{Zn}} \frac{\alpha_{Zn}}{\alpha_{Co}} \frac{\lambda_{Zn}}{\lambda_{Co}}$$

where n_{Co} and n_{Zn} are the numbers of cobalt and zinc atoms, at the surface, I_{Co} and I_{Zn} are the intensities of cobalt and zinc, respectively, α_{Co} and α_{Zn} are the photoionisation cross-sections of the respective elements, λ_{Co} and λ_{Zn} are the escape depths for the respective elements.

In cases where the elements being analysed are present in the same material the escape depth term can be approximated as follows:[13]

$$\frac{\lambda_{Zn}}{\lambda_{Co}} = \left(\frac{E_{Zn}}{E_{Co}}\right)^{0.75}$$

where E_{Co} and E_{Zn} are the kinetic energies of the respective elements.

The surface Co/Zn ratios were thus calculated using eqn. (1).

$$\frac{n_{Co}}{n_{Zn}} = \frac{I_{Co}}{I_{Zn}} \frac{\alpha_{Zn}}{\alpha_{Co}} \left(\frac{E_{Zn}}{E_{Co}}\right)^{0.75} \quad (1)$$

The ratio of the photoionization cross-sections, α_{Zn}/α_{Co}, was taken from Schofield[14] and was found to be 1.499. The kinetic energy values for each element were calculated from the binding energy values of the atom obtained from Briggs and Seah.[12] The ratio was found to be 0.729. It should be noted that using Al-Kα radiation produces interference in the Co $2p_{3/2}$ spectral region (at the lowest binding energies) by an Auger transition, which causes an absolute Co $2p_{3/2}$ integrated intensity to be overestimated by 15%.[15] Absolute binding energies are difficult to determine because of the problems of charge referencing. The determination of quantitative surface analysis is also very difficult, the problems being outlined by Briggs and Seah.[12] Therefore, the aim of this work was not to obtain absolute values, but rather to identify any trends that were present.

Results

Characterisation of the hydroxycarbonate precursors

The results from the atomic absorption analyses of the precursors and oxides are shown in Tables 1 and 3 respectively. The Co/Zn atomic ratios were close to the nominal loadings used and there was good agreement, within experimental error, between the values obtained for the precursors and the oxides. The experimental error for the atomic absorption measurements was ±2%. Microanalysis for C,H,N revealed that no nitrogen was present in the precursors.

The phases detected in the precursors by X-ray diffraction pattern are summarised in Table 1. Precursors with Co/Zn ratios of 0/100 and 10/90 gave diffraction patterns correspond-

Table 1 Summary of AA, XRD and TG data for the precursors

nominal atomic loading	AA			XRD	TG						
					T/°C			mass loss (%)			
	Co (mass%)	Zn (mass%)	calc. Co/Zn	phase detected	surface H_2O	loss of structural H_2O and CO_2	$Co_3O_4 \rightarrow CoO$	150 °C	$\uparrow H_2O + \uparrow CO_2$	residue	$Co_3O_4 \rightarrow CoO$
0/100		54.40		hydrozincite		272		2.0	23.5	2.5	
10/90	5.55	51.78	10/90	hydrozincite		295			23.7	1.2	
20/80	10.41	39.13	23/77	hydrozincite(major) + spherocobaltite(minor)		302	327(sh) 927	2.5	23.5	2.5	2.0
30/70	13.83	35.93	30/70	hydrozincite(major) + spherocobaltite(minor)	70	302	927	8.0	20.5	3.0	2.0
40/60	19.06	28.89	42/58	hydrozincite + spherocobaltite	65	272	310(sh) 940	5.5	24.0	3.0	3.5
50/50	17.11	25.08	43/57	hydrozincite(minor) + spherocobaltite(major)		250	285(sh) 960	5.0	33.5	2.2	2.7
70/30	33.73	12.05	75/25	spherocobaltite		262	925	3.0	23.5	1.7	5.2
90/10	39.24	5.89	88/12	spherocobaltite(major) + porta[a]	70	255	945	14.0	24.0	2.0	4.5
100/0	58.93			Porta[a]		255	955		25.5	3.2	5.0

[a]Ref. 9.

ing exclusively to that of the mineral hydrozincite, $Zn_5(CO_3)_2(OH)_6$.[16] XRD studies of the precursors Co/Zn 20/80, 30/70, 40/60 and 50/50 indicated the presence of both hydrozincite and spherocobaltite, $CoCO_3$,[17] phases, with the spherocobaltite phase becoming more prominent with increasing cobalt loading. Spherocobaltite was the only phase detected for the precursor Co/Zn 70/30. The diffraction pattern for the precursor Co/Zn 90/10 indicated that it comprised predominantly spherocobaltite, but a small amount of a second phase was also observed. This minor phase matched that of the basic cobalt carbonate, $Co(CO_3)_{0.5}(OH)_{1.0}\cdot 0.1H_2O$, reported previously by Porta *et al.*[9] The precursor Co/Zn 100/0 had a diffraction pattern that corresponded exclusively to that of the basic cobalt carbonate described above. No systematic changes in the lattice parameters for hydrozincite or spherocobaltite were detected in any of the precursors. However, the formation of monophasic hydrozincite for the Co/Zn 10/90 precursor, and monophasic spherocobaltite for the Co/Zn 70/30 precursor, may indicate partial solubility of cobalt in zinc and zinc in cobalt respectively, although the existence of amorphous cobalt and zinc phases cannot be discounted entirely.

The TG data obtained for all the precursors are given in Table 1. Temperatures are recorded for the maximum rates for each decomposition step calculated from maxima in the differential traces of the decomposition curves. Mass losses recorded at or below 150 °C were attributed to surface water. The tabulated $\uparrow H_2O + \uparrow CO_2$ refers to mass losses between 150 and 350 °C attributed to simultaneous loss of CO_2 and H_2O, and the residue refers to mass losses from 350 to 900 °C. A single-step decomposition corresponding to that required for the decomposition of hydrozincite to zinc oxide (26.0%) was observed for the Co/Zn 0/100 and 10/90 precursors in accordance with the detection of a single-phase hydrozincite by XRD. The single-step decomposition corresponded to the loss of water and CO_2 simultaneously, as reported previously.[18] The precursor appeared to be stabilised in the presence of cobalt since the decomposition maximum increased from 272 to 295 °C. However, decomposition commenced at a lower temperature in the mixed carbonates. This was probably due to the decomposition of the thermally less stable cobalt carbonate phase. The increase in the decomposition maximum for the biphasic oxides (Co/Zn 10/90 to 30/70) could be attributed to the synergic effect of cobalt and zinc being in intimate contact in the hydrozincite phase. However, at higher cobalt concentrations, the precipitating cobalt ion would preferentially form spherocobaltite which was present as a major phase, reducing the Co–Zn interaction and thus the thermal stability of the precursor. A high-temperature shoulder was observed in the mixed Co/Zn precursors 20/80, 40/60 and 50/50. This indicated that two distinct Co/Zn ratios were present. A large exothermic transition was observed on decomposition of the Co/Zn 50/50 precursor. A single-step decomposition of the precursor to Co_3O_4 was observed for Co/Zn 70/30 and 90/10 and can be attributed to the decomposition of spherocobaltite. Dissolved zinc has little effect on the decomposition of the spherocobaltite phase.

The mass loss observed for the Co/Zn 100/0 precursor is consistent with the decomposition of the basic cobalt carbonate observed by Porta *et al.*[9] All the precursors with Co/Zn ratios $\geqslant$20/80 underwent a further decomposition step centred at *ca.* 930 °C which could be attributed to the decomposition of Co_3O_4 to CoO.[19]

UV–VIS–NIR diffuse reflectance spectra of the precursors Co/Zn 10/90 to 0/100 showed the presence of a band centred at 520 nm and a second broad band with its centre at *ca.* 1300 nm which had a shoulder at 1382 nm. These bands were typical of a Co^{2+} ion ($3d^7$ electronic configuration) in octahedral symmetry.[9,20] The band at 520 nm can be assigned to the transition $^4T_{1g}(F)\rightarrow{}^4T_{1g}(P)$, whilst the band at *ca.* 1300 nm can be assigned to the $^4T_{1g}(F)\rightarrow{}^4T_{2g}(F)$ transition. The position of the centre of this broad band increased as the cobalt percentage increased.

The FTIR spectra for all of the precursors exhibited the characteristic vibrational modes of the carbonate group at 1509, 1385, 1045 and 835 cm^{-1}.[11] The stretching and bending modes of H_2O were observed at 3400 and 1630 cm^{-1}. Bands specific to hydrozincite and spherocobaltite were observed for Co/Zn 0/100 and 100/0 in the 'fingerprint' region (400–1100 cm^{-1}).[21] For the intermediate loadings a strong sharp band appeared at 840 cm^{-1} and became more intense with further increases in cobalt loading. This band was also present in $CoCO_3$ but was broad and of low intensity.

TEM studies revealed that all the precursors were of a crystalline nature. Electron diffraction data were in accord with powder diffraction results, *i.e.* hydrozincite and/or spherocobaltite phases were detected, depending on the Co/Zn ratios. The Co/Zn 100/0 precursor gave electron diffraction data which were in very good agreement with the phase detected by Porta *et al.*,[9] again agreeing with the XRD results. Selected electron micrographs are shown in Fig. 1. The Co/Zn 0/100 and 10/90 samples consisted of a single hydrozincite phase [Fig. 1(a)] whereas the Co/Zn 100/0 precursor was entirely comprised of Porta's basic cobalt carbonate $Co(CO_3)_{0.5}(OH)_{1.0}\cdot 0.1H_2O$[9] [Fig. 1(d)]. Other Co/Zn ratios gave rise to two phases. This is particularly clear in Fig. 1(b) which represents the typical morphology of the Co/Zn 20/80 sample. Hydrozincite crystals similar to those in Fig. 1(a) can be seen in the lower part of the micrograph together with the more 'sponge-like' morphology found for spherocobaltite. The hydrozincite phase in all samples was very susceptible to decomposition to ZnO under electron beam irradiation.

Surface analysis of each of the precursors was carried out by XPS. Selected narrow energy scans of the Zn $2p_{3/2}$ and Co $2p_{3/2}$ photoelectron peaks of the precursors are shown in Fig. 2 and 3 respectively. The photoemission energies for zinc, cobalt and oxygen are reported in Table 2.

It can be seen that the $2p_{3/2}$ transition for zinc for each precursor consisted of only a single peak, at $E_B \approx 1022.0$ eV. The presence of the low binding energy feature at $E_B \approx 1019.6$ eV is caused by the highly focused M-probe electron source reducing the ion to its metallic state. The Co $2p_{3/2}$ peak, positioned at $E_B \approx 781.0$ eV, consisted of a main peak with a satellite peak at a higher binding energy, $E_B \approx 785.8$ eV. The values of the binding energies and the presence of the satellite peak for the Co $2p_{3/2}$ transition were typical of zinc and cobalt in the 2+ oxidation state.[12,22,23] The O 1s transition at $E_B = 531.0$ eV was similar to that expected for oxygen in CO_3^{2-}.[24]

It has been reported that for Co^{2+}-containing compounds the satellite–main peak energy separation increases and the satellite/main peak intensity ratio decreases with increasing covalent character of the metal–ligand bond.[25] Applying this to the Co–Zn precursor data (see Table 2), it could be seen that the satellite–main peak energy separation decreased as the cobalt loading increased. This was accompanied by an increase in the satellite/main peak intensity ratio for the mixed metal precursors with a Co/Zn ratio of $>$30/70. This suggested that there was an increase in the ionic character of the chemical bonding around the Co^{2+} ions for the mixed Co/Zn precursors with increasing cobalt concentration.

The peak shapes of the zinc and cobalt transitions were very similar for all the precursors. The main binding energy positions of Zn $2p_{3/2}$ and Co $2p_{3/2}$ varied from 1021.5 to 1022.6 eV and from 780.9 to 781.5 eV respectively. This inconsistency probably resulted from the variable nature of the CO_3^{2-}/OH ratio fixed during the precipitation process.

The surface Co/Zn atomic ratios were derived from the peak intensity ratios of the $2p_{3/2}$ transition. The relationship between atomic ratios at the surface (XPS, $2p_{3/2}$) and the bulk (AA) are shown in Fig. 4. There was a $\pm$5% error associated with

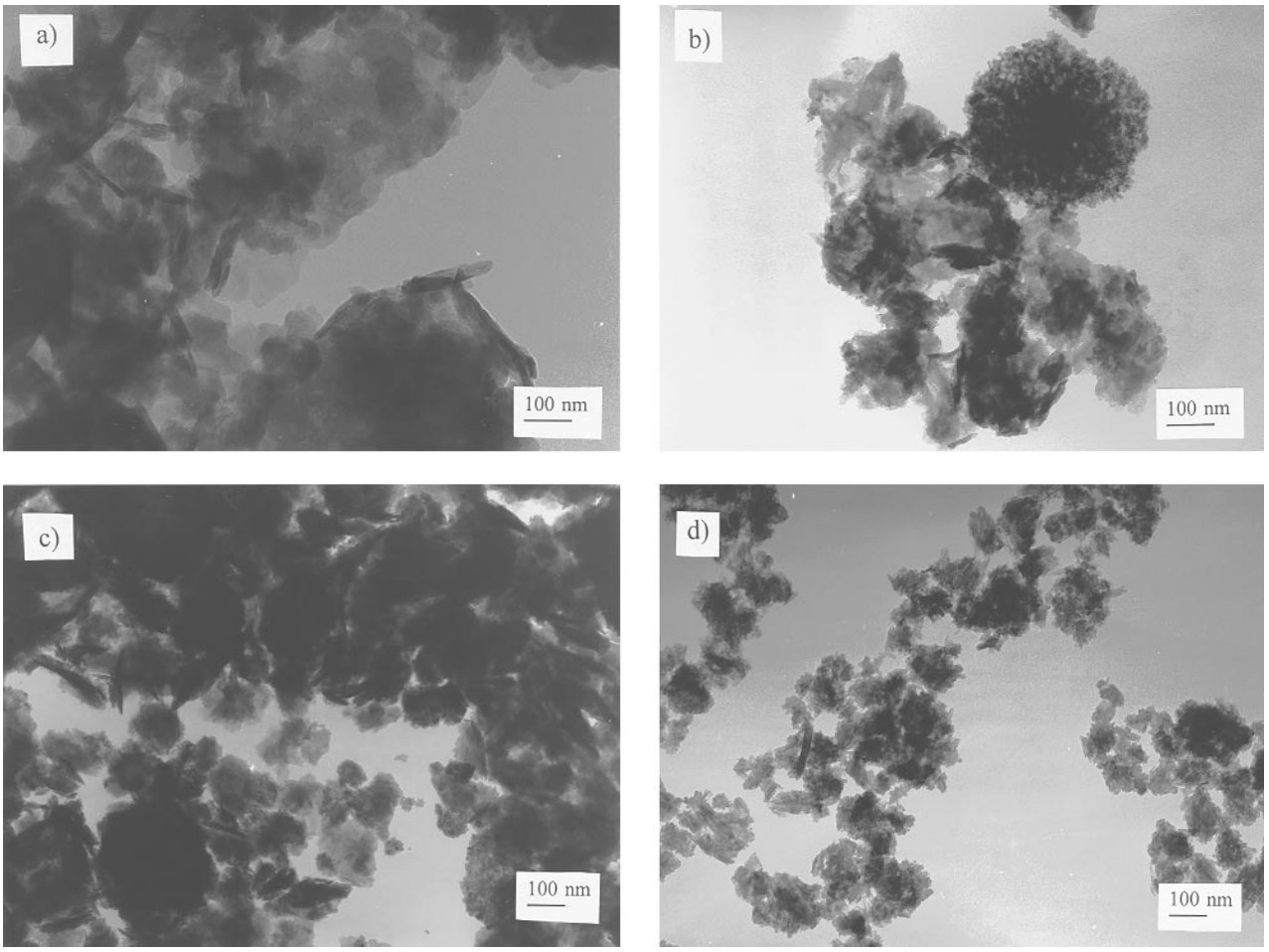

Fig. 1 Transmission electron micrographs of the hydroxycarbonate precursor phases of Co/Zn: (a) 0/100, (b) 20/80, (c) 40/60, (d) 100/0

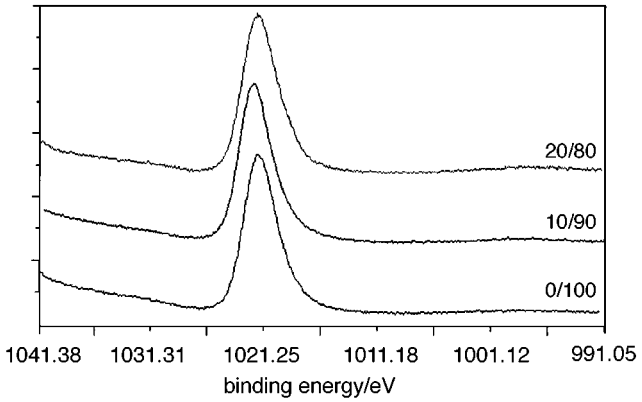

Fig. 2 Typical examples of the zinc $2p_{3/2}$ transition for the hydroxycarbonate precursors. The intensities have been normalised.

the integrated XPS data and error bars based on these measurements have been included in Fig. 4. The straight line (slope = 1) represents a homogeneous distribution of the Co/Zn ratio between the surface and the bulk. The data showed that there was no evidence of significant cobalt enrichment at the surfaces of these precursors.

In order to investigate further the surface Co/Zn ratio, the 10/90, 30/70 and 50/50 precursors were ground finely and the spectra collected under identical conditions. The binding energies for the ground precursors are listed in Table 2 and their surface Co/Zn ratios are presented in Fig. 4. The ground precursors of Co/Zn composition 10/90, 30/70 and 50/50 are referred to as 10/90G, 30/70G and 50/50G respectively in Table 2 and Fig. 4. The plot of Co/Zn surface composition *vs.* bulk composition (Fig. 4) showed that for the 30/70 and 50/50 ground samples there was a lowering of the Co/Zn ratio on the surface compared with their unground counterparts, whereas there was a small increase in the ratio for the ground 10/90 precursor. This suggested that the particles had zinc-rich cores and that a more homogeneous distribution of the cobalt and zinc between the bulk and the surface resulted due to the particles continually shearing/reforming during the grinding process.

Characterisation of the oxides

The hydroxycarbonate precursors were decomposed by thermal treatment at 350 °C for 16 h in air. The XRD patterns for all the samples showed the presence of broad, well defined peaks. This suggested that crystalline oxides of small average particle size were formed. The oxide phases formed at each nominal loading are summarised in Table 3.

The XRD patterns for Co/Zn 0/100cal and 100/0cal were similar to the JCPDS patterns for ZnO[26] and Co_3O_4[27] respectively. The Co/Zn 10/90cal sample gave a pattern which corresponded to that of ZnO. It is likely that a monophasic cobalt-containing solid solution of zinc oxide was formed since no extra peaks were found, although the presence of some amorphous material cannot be discounted entirely. The 70/30cal and 90/10cal samples gave a monophasic pattern corresponding to a cobalt oxide phase, indicating that all the zinc was probably in the form of a solid solution in the cobalt oxide. The oxides 20/80cal, 30/70cal, 40/60cal and 50/50cal had interplanar spacings in their diffraction patterns corresponding to zinc oxide and a 'cobalt oxide type' phase which may either have been Co_3O_4, or the zinc spinel, $ZnCo_2O_4$.[28] It was not possible to identify which phase was present as the diffraction patterns

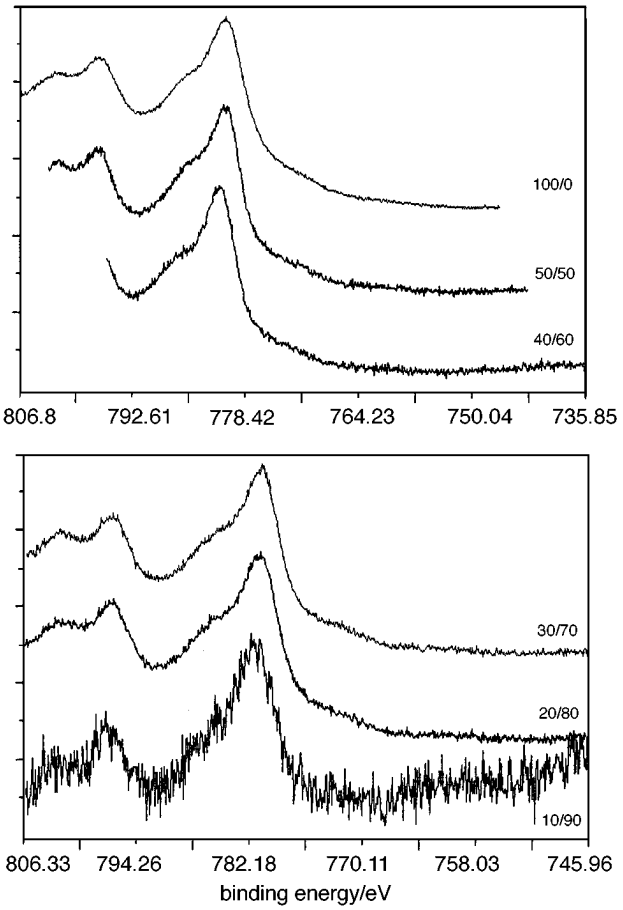

Fig. 3 Cobalt $2p_{3/2}$ transition for the hydroxycarbonate precursors. The intensities have been normalised.

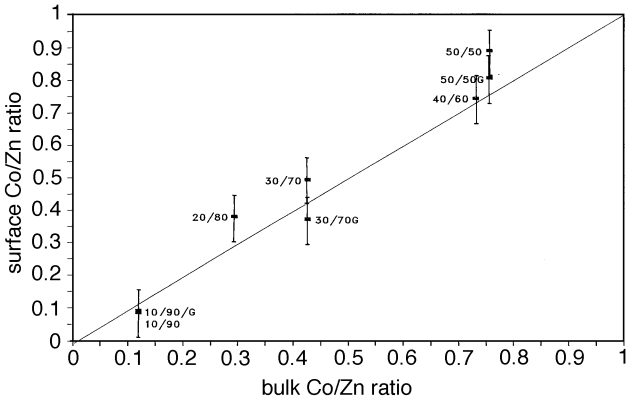

Fig. 4 Co/Zn composition at the surface (XPS, $2p_{3/2}$) and in the bulk (AA) for the precursors

for Co_3O_4 and $ZnCo_2O_4$ are very similar and the cobalt oxide type phase in the samples showed consistent differences in position from the literature values. Co_3O_4 will be given as the literature comparison here and in subsequent sections. The positions of a number of peaks of the cobalt oxide type phase were measured and compared to the literature values of Co_3O_4 (Table 4). Only peaks which had no interference from ZnO were selected. The peaks for the cobalt oxide type phase occurred at lower values of 2θ than the reference phase in each sample. The shifts in position of the *d*-spacings suggested that the lattice of the cobalt oxide type phase had expanded. This expansion suggests that Zn^{2+} ions were dissolved in the cobalt oxide type phase. The zinc oxide phase matched the reference pattern very well and was used as an internal standard, confirming that the shift in position of the cobalt oxide type phase was a real effect and not a function of the sample preparation. It seems most likely that the phase present was $Zn_xCo_{3-x}O_4$ ($x \leqslant 1$). The phases detected are summarised in Table 3.

A qualitative measure of the relative proportions of the phases in each sample was obtained from the peak intensities. The intensities of the Co_3O_4 peaks at $d = 2.02$ and 1.56 Å were selected as they do not overlap with the ZnO peaks. The intensities were found to increase as the percentage of cobalt increased. This suggested that the relative amounts of the cobalt oxide type phase increased with increasing cobalt loading. The results are summarised in Table 3. The amount of cobalt oxide type phase for the biphasic loadings is indicated on a scale of 1 to 4 with 1 indicating that is a minor phase and 4 indicating that it is a major phase.

TEM again confirmed the presence of the phases detected by XRD. In addition, the selected area diffraction technique revealed, in the Co/Zn 10/90cal sample, that although ZnO was the predominant phase there were also some very weak

Table 2 Binding energies for the precursors and finely ground precursors. Charging effects have been referenced to the C 1s peak of the carbonate group at $E_B = 289.1$ eV (FWHM given in parentheses)

	Zn $2p_{3/2}$ E_B/eV	Co $2p_{3/2}$ E_B/eV	E_{sep}[a]/eV	ratio sat./main	O 1s E_B/eV	C 1s E_B/eV
0/100	1021.9(2.9)				531.2(2.9)	289.1(2.5)
	1019.6(3.8)				528.2(2.6)	284.2(2.9)
10/90	1022.4(2.9)	781.5(4.9)	4.95	0.40	531.1(2.9)	289.1(2.4)
	1019.9(3.7)	786.4(5.3)			528.5(2.6)	284.3(3.1)
20/80	1022.0(3.1)	781.0(4.4)	4.87	0.46	531.2(2.8)	289.1(2.8)
	1019.4(3.1)	785.8(5.2)			530.0(2.9)	284.2(3.4)
30/70	1021.5(3.1)	780.9(4.3)	4.77	0.45	531.0(3.0)	289.1(2.7)
	1018.8(2.8)	785.6(4.9)			528.6(3.4)	284.3(3.2)
40/60	1022.6(2.9)	780.9(4.0)	4.60	0.53	531.2(2.9)	289.1(2.4)
	1020.4(3.0)	785.4(5.4)			529.0(3.1)	283.4(4.6)
50/50	1021.7(2.9)	780.9(4.2)	4.55	0.58	531.1(2.8)	289.1(2.6)
	1019.5(3.3)	785.4(5.4)			528.6(2.7)	284.1(3.2)
100/0		781.0(5.4)	5.31	0.22	531.2(3.1)	289.1(2.6)
		786.3(4.2)			528.7(3.7)	284.3(4.1)
10/90G	1021.4(2.8)	781.1(4.1)			531.1(2.9)	289.1(2.6)
	1019.0(3.5)	785.7(3.7)			528.9(3.0)	284.3(3.3)
30/70G	1021.9(3.4)	781.4(4.9)			531.1(3.2)	289.1(2.4)
	1019.3(4.8)	786.4(4.6)			528.7(3.8)	283.9(5.0)
50/50G	1022.0(3.0)	781.2(3.8)			531.7(3.1)	289.1(2.9)
	1019.5(4.1)	785.6(5.6)			528.7(2.8)	284.3(3.3)

[a]Satellite–main peak energy separation.

Table 3 Summary of AA, XRD, TEM and BET data for the oxides

nominal atomic loading	Co (mass%)	Zn (mass%)	calc. Co/Zn	phases present	particle sizes/nm	S/ $m^2\ g^{-1}$
0/100		79.97		ZnO	40–80	38.8
10/90	6.79	63.36	11/89	ZnO	20–50	45.1
20/80	18.66	59.26	26/74	ZnO(major)+Co_3O_4(minor,1)	10–20	64.9
30/70	21.69	53.39	31/69	ZnO(major)+Co_3O_4(minor,2)	—	68.2
40/60	29.13	40.36	44/56	ZnO(minor)+Co_3O_4(major,3)	10–20	66.4
50/50	31.69	40.67	46/54	ZnO(minor)+Co_3O_4(major,4)	5–15	59.7
70/30	43.80	16.42	75/25	Co_3O_4	—	56.5
90/10	64.74	7.16	91/9	Co_3O_4	—	82.9
100/0	69.46			Co_3O_4	10–20	87.1

Table 4 Variations of d-spacings of the cobalt oxide type phase

nominal Co/Zn	(400) peak of Co_3O_4 phase[a]		(511) peak of Co_3O_4 phase[a]	
	2θ/degrees	d-spacing/Å	2θ/degrees	d-spacing/Å
Co_3O_4[b]	52.578	2.021	70.240	1.556
20/80	52.40	2.027	70.00	1.561
30/70	52.10	2.038	69.80	1.564
40/60	52.10	2.038	69.60	1.578
50/50	52.20	2.035	69.80	1.564

[a] The peaks at $2\theta = 52.578°$ and $70.240°$ are the (400) and (511) reflections respectively. These peaks were selected as there is no interference from zinc oxide. [b] Ref. 27.

rings corresponding to a cobalt oxide type phase. Micrographs of selected oxides are shown in Fig. 5. The particle sizes of the metal oxide particles were measured and the data are listed in Table 3. Smaller particles were observed in the Co-doped ZnO than in ZnO itself. In general, the oxides consisted of fused crystallites and conglomerates of these, as shown for example in Fig. 5(c). The best formed, most discrete crystals were found in the Co/Zn 100/0cal and 0/100cal samples.

UV–VIS–NIR diffuse reflectance spectroscopic characterisation was used to determine the geometry and oxidation state of the cobalt in the cobalt-containing oxides. All the samples at cobalt loadings >10% were black owing to Co^{2+}–Co^{3+} charge-transfer absorption extending across the whole of the visible region.[29] However, absorption bands were observed overlying the intervalence charge-transfer background. The spectrum for the Co/Zn 100/0cal sample contained bands at 356 and 729 nm which could be assigned to the transitions $^1A_{1g}(I) \rightarrow {}^1T_{2g}(I)$ and $^1A_{1g}(I) \rightarrow {}^1T_{1g}(I)$ respectively for a Co^{3+} ion in octahedral symmetry.[30] A further broad band was observed at *ca.* 1300 nm, which could be assigned to the transition $^4A_2(F) \rightarrow {}^4T_{1g}(F)$ for a Co^{2+} ion in tetrahedral symmetry.[11] These transitions would be expected for the normal spinel Co_3O_4, which has Co^{2+} tetrahedrally coordinated and Co^{3+} octahedrally coordinated. The spectra for the mixed oxides with Co/Zn ratios >50/50 were similar to those described above for Co/Zn 100/0, but at lower cobalt concentrations the only bands/absorption edges that could be attributed to cobalt were those due to the intervalence charge-transfer background. The Co/Zn 0/100cal sample had an absorption edge at *ca.* 380 nm which could be assigned to ZnO.[11] This edge was also observed in samples with Co/Zn <30/70, but with diminishing intensity with increasing cobalt loading.

FTIR spectra of the oxides all showed the presence of the OH stretch at *ca.* 3400 cm^{-1} and the OH bending mode at *ca.* 1625 cm^{-1} indicating that the surfaces were hydroxylated. A band at *ca.* 1510 cm^{-1} was also observed. This was considerably reduced in size compared with that observed in the precursors and could be attributed to residual carbonate. This is in accordance with the TG results which showed that the last traces of carbonate are not removed until *ca.* 900 °C. The IR spectrum for Co/Zn 0/100cal also contained an intense, broad peak at 550 cm^{-1} which could be attributed to ZnO.[31] This peak decreased in intensity with increasing cobalt loading and was replaced by two sharp bands at *ca.* 588 and 575 cm^{-1} which could be attributed to the presence of Co_3O_4.[21]

The surface areas of all the oxides are listed in Table 3. The lowest surface area was attained from the decomposition of the hydrozincite precursor. An increase in surface area was obtained on decomposition of the biphasic (hydrozincite+spherocobaltite) precursors to ZnO and the cobalt oxide type phase in accordance with the decrease in particle size observed for the biphasic oxides compared with ZnO. Decomposition of the basic cobalt carbonate formed the oxide with the highest surface area.

All the oxides were analysed by XPS to see if the surface properties mirrored those of the bulk. The Zn $2p_{3/2}$ XP spectrum of the Co/Zn 0/100cal sample is shown in Fig. 6. All the oxides showed similar spectra. Their shapes and binding energies, $E_B \approx 1021.6$ eV (see Table 5), was typical of Zn in a 2+ oxidation state.

The Co $2p_{3/2}$ XP spectra for all the oxides are shown in Fig. 7. For Co/Zn 100/0cal the Co $2p_{3/2}$ main peak was at $E_B = 780.3$ eV with the Co $2p_{3/2}$–$2p_{1/2}$ spin–orbit splitting equal to 15.1 eV. Peak fitting using Gaussian curves gave binding energies of 780.1 and 782.1 eV for the Co^{3+} and Co^{2+} ions respectively. This was in agreement with Chuang *et al.* for their assignments of a high-purity Co_3O_4 powder.[32] As the cobalt loading decreased, the photoelectron peak indicating the presence of the Co^{2+} ion decreased in intensity. Only the Co^{3+} ion was present for Co/Zn 30/70cal and lower loadings (see Fig. 7). This indicated that at low cobalt loadings the normal spinel $ZnCo_2O_4$ may be formed at the surface. Fig. 7 also indicates that the background step increased as the cobalt loading increased. This was deduced from the step size of the baseline between the low and high binding energies of the peak (see Table 5). The background step was caused by inelastic collisions of the emitted photoelectron which created an increasing signal level between the high and low binding energies of the photoelectron peak. This is illustrated in Fig. 8. It shows that for a small increase in the background step all the signal originated from the outermost surface. As this step after photoemission gets bigger it shows that some of the electrons detected are also coming from further inside the 'bulk'. The lower the step the greater the contribution of the surface ions to the signal. A step-size increase would be expected due to the increase in the cobalt concentration at the higher Co/Zn ratios.

The surface Co/Zn atomic ratios were derived from the peak intensity ratios of the $2p_{3/2}$ transition for the calcined precursors and are plotted against the bulk (AA) results in Fig. 9. The error bars associated with the $2p_{3/2}$ derived ratios for the calcined precursors are shown in Fig. 9. Bearing in mind the inherent difficulties associated with quantitative surface analysis[12] and the ±5% error associated with the integrated XPS

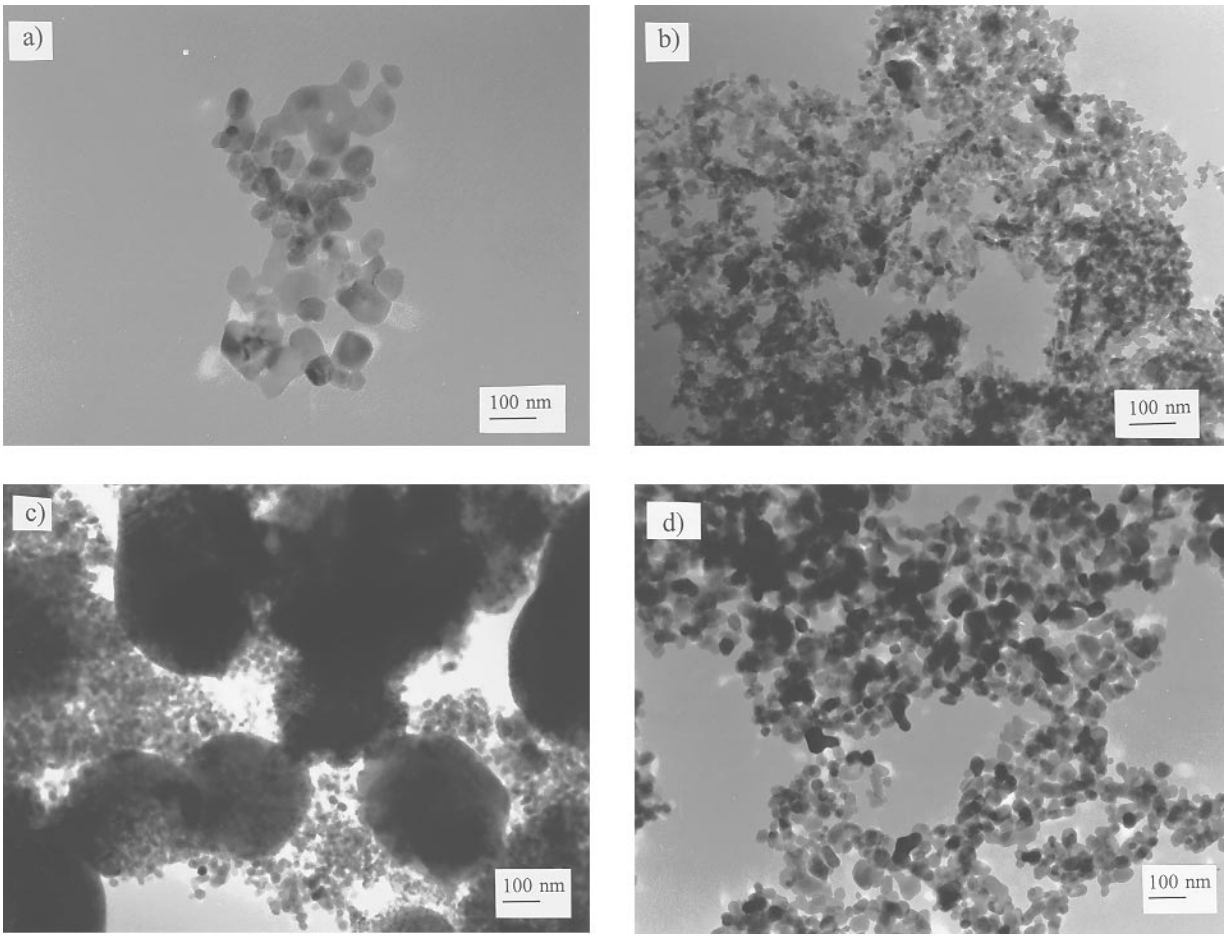

Fig. 5 Transmission electron micrographs of the oxide phases of Co/Zn: (a) 0/100, (b) 20/80, (c) 50/50, (d) 100/0

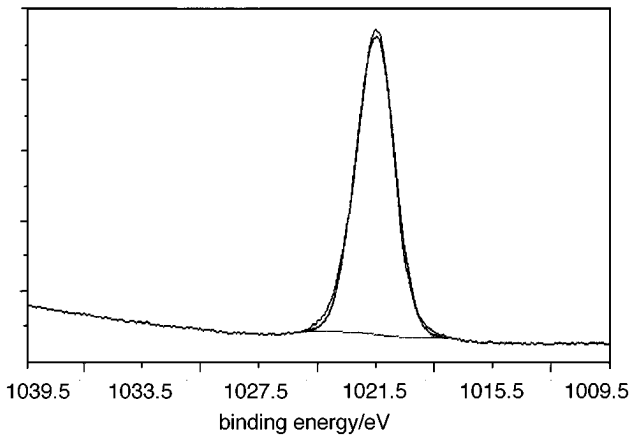

Fig. 6 The Zn $2p_{3/2}$ transition for the Co/Zn 0/100 oxide (calcined at 350 °C, 16 h). It is typical (in shape and position) of the other loadings.

data, it can be concluded that, as for the precursors, there was no evidence for significant enrichment of cobalt at the surface of the oxides.

With the exception of the Co/Zn 10/90cal sample the zinc and cobalt ions in the mixed Co/Zn systems gave a second and third distinct region at lower binding energies, separated by *ca.* 3 eV. They were most apparent for the 20/80, 30/70 and 40/60 loadings. This low binding feature, which was seen at $E_B \approx 1018.8$ eV for zinc ions and at $E_B \approx 777.7$ eV for cobalt ions, was the result of the metal ions at the surface of a solid being reduced by the highly focused M-probe XPS source to their respective metallic forms.

The O 1s spectra of the oxides were all very similar in shape. The spectra were curve-fitted into two Gaussians curves and the main peak binding energy was fixed at $E_B = 530.0$ eV. The second feature at higher binding energy, $E_B = 532.2$ eV, was most likely to be due to the presence of a hydroxy species at the surface.

To investigate further the effect of the calcination process, the precursors with nominal Co/Zn concentrations of 10/90 and 50/50 were calcined at various temperatures between 100 and 700 °C for 8 h. These ratios were chosen as they are at the extremes of the cobalt loadings in the mixed samples under investigation.

The Zn $2p_{3/2}$ binding energies varied slightly for both loadings within each series but are in accordance with literature values for zinc in the 2+ oxidation state. The XP spectra of the Co $2p_{3/2}$ transition for the 10/90 series are shown in Fig. 10. At temperatures below 350 °C the Co $2p_{3/2}$ transition consisted of a main peak, positioned at $E_B \approx 781.7$ eV, with a satellite peak at higher binding energy, $E_B \approx 787.7$ eV. This is typical of a Co^{2+} ion. The signal to noise ratio of the spectra increased noticeably as the calcination temperature was increased. At 350 °C and above, peak fitting of the Co $2p_{3/2}$ peak revealed the presence of the Co^{3+} ion, $E_B = 779.9$ eV, with only a very small contribution from the Co^{2+} ion, $E_B = 782.6$ eV, and its corresponding shake-up satellite.

The Co $2p_{3/2}$ spectra for the 50/50 series indicate that these samples behaved similarly to the 10/90 series. Calcination at < 200 °C gave a Co $2p_{3/2}$ transition which from peak shape and binding energy was characteristic of the presence of Co^{2+} ions. The photoelectron peak obtained after calcination at temperatures between 200 and 400 °C was peak-fitted and this indicated the presence of a Co^{3+} component, $E_B = 780.0$ eV, and a very small contribution from a Co^{2+} component, $E_B = 782.0$ eV. However, at 480 °C and above, only the Co^{3+} ion was present.

Table 5 Binding energies for the oxides. Charging effects have been referenced to the O 1s peak at $E_B = 530.0$ eV (FWHM in parentheses)

Co/Zn	Zn $p_{3/2}$ E_B/eV	Co $2p_{3/2}$ E_B/eV	O 1s E_B/eV	e$^-$ count difference[a]	$E_B(Zn^{2+}) - E_B(Zn^0)$	$E_B(Co^{2+}) - E_B(Co^0)$	$E_B(Co^{3+}) - E_B(Co^0)$
0/100	1021.46(2.36)		530.0(2.1)		—	—	—
			531.9(2.1)				
10/90	1021.2(3.2)	779.4(3.4)	530.0(3.2)	1594	—	—	—
20/80	1021.4(3.8)	778.9(3.2)	530.0(3.6)	4213	3.1	—	1.3
	1018.3(4.1)	777.6(4.2)	532.4(3.0)				
30/70	1021.7(3.7)	780.1(3.9)	530.0(4.1)	5209	3.0	—	2.0
	1018.7(3.2)	778.1(3.9)					
40/60	1021.7(3.2)	782.4(2.5)	530.0(2.3)	5995	2.8	4.8	2.8
	1018.9(2.6)	780.4(2.6)	532.2(2.4)				
		777.6(1.5)					
50/50	1022.0(3.0)	782.4(2.6)	530.0(2.5)	10593	2.6	4.8	2.8
	1019.4(1.7)	780.3(2.9)	532.4(2.0)				
		777.6(1.5)					
100/0		782.1(2.6)	530.0(2.3)	17799	—	4.8	2.8
		780.1(2.9)	532.2(2.7)				
		777.3(1.0)					

[a]Difference in electron count between the high and low binding energies for the Co $2p_{3/2}$ peak.

Quantitative analyses for the 10/90 and 50/50 series are shown in Table 6. For both series there was a variation in the surface Co/Zn ratios for the samples calcined at temperatures below 350 °C. However, above 350 °C the surface Co/Zn ratios were closer to the expected values, *i.e.* 0.1 and 0.5 for the 10/90 and 50/50 series respectively. This suggested that no significant segregation of cobalt to the surface occurred as the calcination temperature was increased above 350 °C.

For both series of loadings the variation in the binding energies and the Co/Zn atomic ratios at the surface for the samples calcined at <350 °C is most likely to be due to variations in the concentrations of carbonate and hydroxy groups at the surface of the sample as decomposition of the precursors took place. At temperatures above 350–400 °C, where the decomposition process was thought to be nearing completion, there was only a small variation in the surface Co/Zn ratios and the binding energies for the Zn $2p_{3/2}$ and Co $2p_{3/2}$ peaks became more consistent.

The true ionic charges in many transition-metal oxides are less than those predicted from formal oxidation states. Siegbahn *et al.*[33] showed that, using eqn. (2), the chemical shift, δ, determined from XPS data of an ion with respect to that atom with zero charge could be used to calculate the true ionic charge of the ion,

$$\delta = E_B^{q_c} - E_B^{0} = q_c\left(\frac{1}{r} - \frac{\phi}{R}\right) \quad (2)$$

where r is the ionic radius, ϕ/R is the self-potential and $E_B^{q_c}$ and E_B^{0} are the binding energies of atoms of charge q_c, the true ionic charge, and zero charge respectively. This theory has been developed further by a number of authors.[34] Problems arise in the calculation of q_c owing to the use of the lattice self-potentials of bulk ions in a calculation which involves surface ions. Because of these limitations the ionic charge obtained is at best qualitative and should only be used for comparison of ionicity among similar solids. In this paper, however, the true ionic charges could not be calculated because of a lack of specific data. However, the shift in the binding energy between the metal and the ion is directly proportional to q_c such that the greater the shift in binding energy the greater the value of q_c. Owing to the highly reducing environment created by many X-ray probes, reduced metal will be present alongside the ions of interest. Presumably since both the metal ion and metal atom are embedded in the same solid matrix, their extra-atomic relaxation effects should be the same.[35] The final state extra-atomic relaxation affects the kinetic energy of the escaping photoelectron due to the relaxation of the electron in the lattice surrounding the ion in response to removal of the photoelectron from the ion. The analysis data are shown in Table 5. The true cation charges of both zinc and cobalt ions show trends across the series. It can be seen that the true cation charge of the Zn^{2+} ions decreased slowly as the cobalt loading was increased. In contrast, the true cation charge with respect to the Co^{3+} ions increased rapidly to a plateau for nominal Co/Zn ratios of 40/60 and above. Also, at Co/Zn 40/60 the presence of the Co^{2+} ions became apparent and it was observed that the ionic charge remained constant as the cobalt loading increased.

Discussion

Coprecipitation can be seen to give a range of precursors depending on the Co/Zn ratio. It is likely that the hydroxide,

Table 6 Quantitative analyses for 10/90 and 50/50 series calcined at various temperatures

	10/90		50/50	
T^a/°C	Co $2p_{3/2}$/Zn $2p_{3/2}$	Co_xZn_{1-x}	Co $2p_{3/2}$/Zn $2p_{3/2}$	Co_xZn_{1-x}
100	0.063	0.074	0.430	0.353
170	0.023	0.028	0.276	0.258
200	0.035	0.042	0.567	0.419
250	0.024	0.029	0.038	0.066
310	0.034	0.041	0.700	0.470
355	0.094	0.106	0.732	0.482
400	0.094	0.106	0.728	0.480
480	0.116	0.128	0.838	0.515
575	0.156	0.165	0.761	0.491
700	0.112	0.124	0.621	0.441

[a]Calcination temperature.

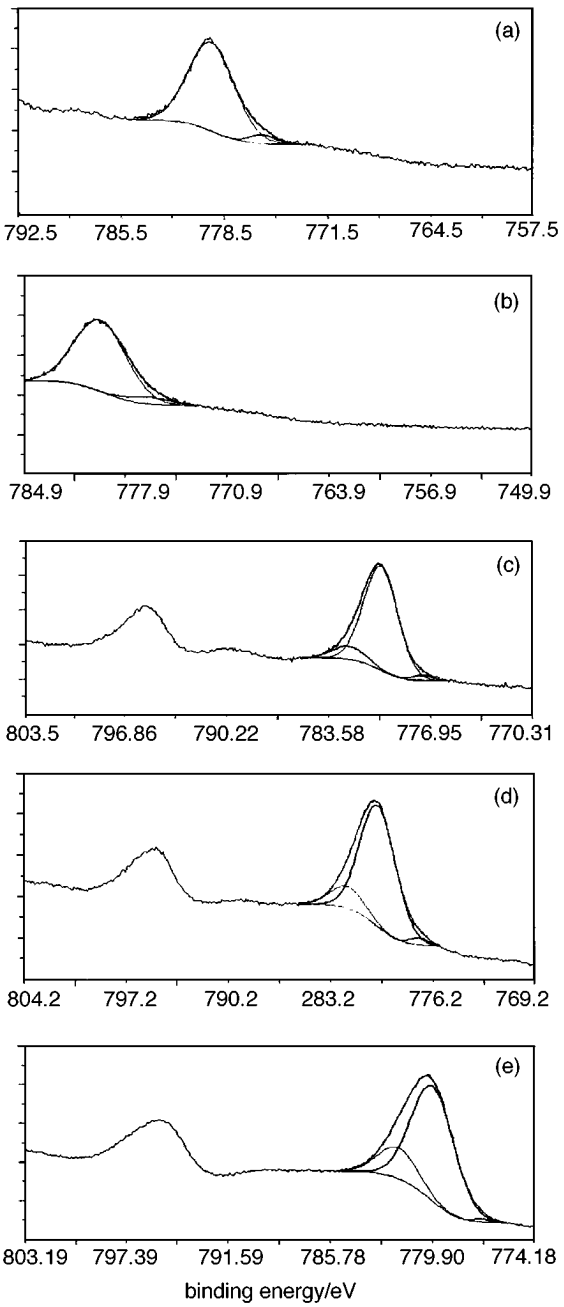

Fig. 7 The Co $2p_{3/2}$ transition for the oxides (calcined at 350 °C, 16 h). The transitions for nominal Co/Zn loadings of (a) 20/80, (b) 30/70, (c) 40/60, (d) 50/50 and (e) 100/0 are shown. Peak fitting showed the presence of Co^{2+} ions $E_B \approx 779$ eV, Co^{3+} $E_B \approx 781$ eV and reduced Co $E_B \approx 777$ eV.

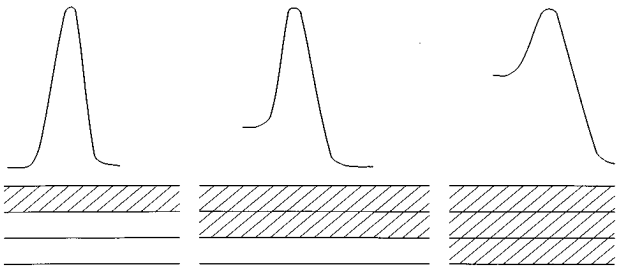

Fig. 8 Diagram of the effect of increasing penetration of cobalt into the bulk on the step-size increase of the Co $2p_{3/2}$ transition

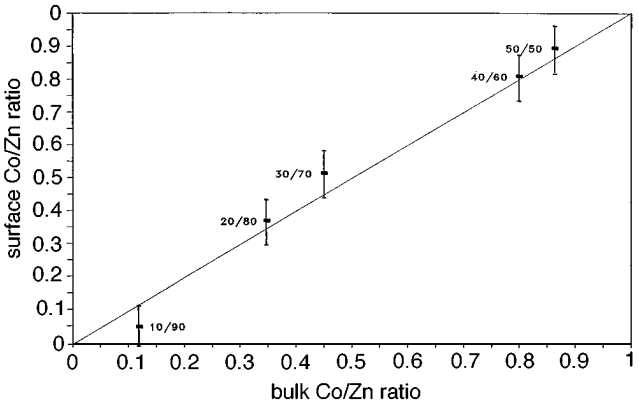

Fig. 9 Co/Zn composition at the surface (XPS, $2p_{3/2}$) and in the bulk (AA) for the oxides. The straight line (slope = 1) represents a homogeneous distribution between surface and bulk.

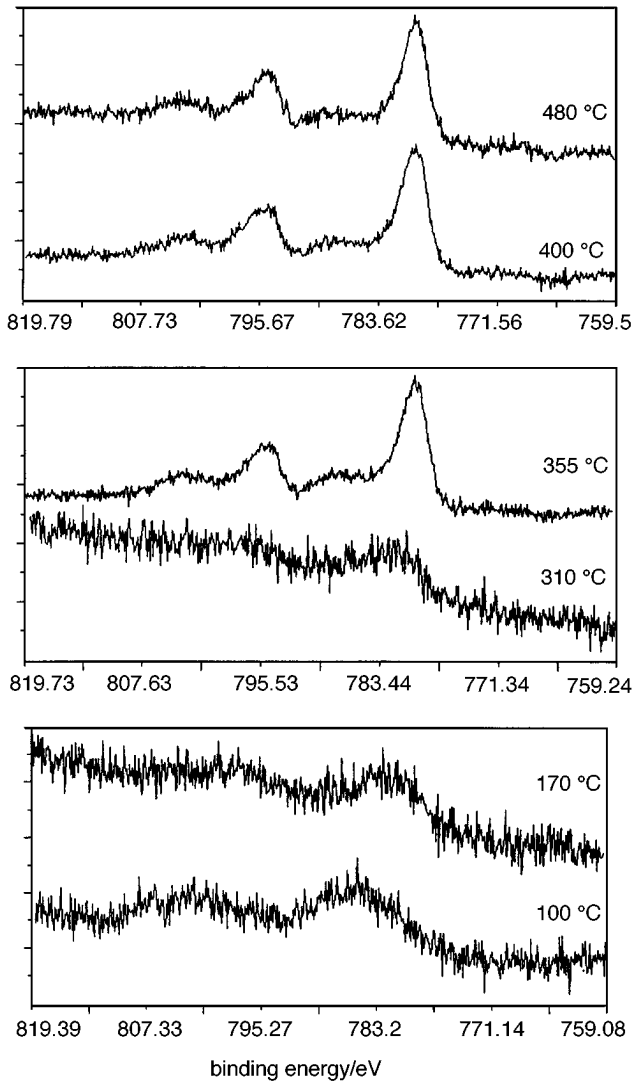

Fig. 10 Cobalt $2p_{3/2}$ transition for Co/Zn 10/90 series (calcined at the temperatures indicated). The intensities have been normalised.

rather than the carbonate, would be precipitated out in a heterogeneous nucleation process following supersaturation on addition of base to the metal salts, since the metal hydroxides have lower solubility products.[36] The precipitate is likely to be predominantly $Zn(OH)_2$ in the initial stages of precipitation, since $Zn(OH)_2$ has a lower solubility product than $Co(OH)_2$. Furthermore, precipitation of $Co(OH)_2$ will take place from the metastable supersaturation region since $Zn(OH)_2$

precipitates at pH 5.2 whereas $Co(OH)_2$ precipitates at 6.8.[37] Precipitation of $Co(OH)_2$ would therefore be less favourable. In practical terms, however, the precipitation process is likely to be less clearly defined since the presence of cobalt would change the precipitation characteristics of zinc, resulting in some entrainment of cobalt particles within the zinc matrix.[7] Crystal growth would then commence on these zinc-rich mixed metal hydroxide nuclei. For mixed metal precursors forming the hydrozincite phase, the Zn^{2+} concentration in solution would decrease as the hydrozincite crystals grew until eventually precipitation of Co^{2+} would be favoured over that of Zn^{2+}, and this would result in an increase in concentration of the cobalt. Two distinct Co/Zn ratios were indicated by a shoulder on the decomposition curve for the TG traces of the mixed precursors. These two Co/Zn ratios may have resulted from the initial preferential nucleation of $Zn(OH)_2$ nuclei which is superseded by $Co/Zn(OH)_2$ precipitation.

Hydrozincite could then be formed through anion exchange:

$$5Zn_{1-x}Co_x(OH)_2 + 2CO_3^{2-} \rightarrow Zn_{5-5x}Co_{5x}(CO_3)_2(OH)_6 + 4OH^-$$

The formation of spherocobaltite was probably preceded by the formation of a zinc-containing $Co(OH)_2$. On the basis of this proposed anion-exchange mechanism, it is likely that the zinc would provide nucleation points for the rapid precipitation of $Co(OH)_2$ which would then undergo ion exchange to form spherocobaltite, *i.e.*

$$Co_{1-x}Zn_x(OH)_2 + CO_3^{2-} \rightarrow Co_{1-x}Zn_xCO_3 + 2OH^-$$

This is supported by the fact that in the absence of zinc, *i.e* in the case of Co/Zn 100/0, precipitation of $Co(OH)_2$ from the metastable supersaturation region occurs more slowly and less efficiently, resulting in a lower yield of hydroxide and incomplete anion exchange to form the cobalt hydroxycarbonate described by Porta, *i.e.* $Co(CO_3)_{0.5}(OH)_{1.0} \cdot 0.1H_2O$.[9]

UV–VIS–NIR diffuse reflectance studies showed that cobalt occupied exclusively the octahedral sites in the hydrozincite structure and XPS analyses revealed that substitution of cobalt also increased the ionic character of the structure. The monoclinic hydrozincite structure is comprised of complex zinc-containing sheet structures which are linked by carbonate groups. Zinc atoms occupy both octahedral and tetrahedral positions in the ratio 3:2. Each carbonate group binds the complex sheets together in a three-dimensional network by sharing one oxygen with a corner of the zinc tetrahedron occurring away from the sheet and another with a corner of the zinc octahedron occurring in the next sheet above. The third oxygen atom of the carbonate is hydrogen bonded to three hydroxy groups.[38] Cobalt replaces zinc in some of the octahedral sites in the hydrozincite structure, increasing both its thermal stability and the ionic character of the bonding. Incorporation of zinc in the rocksalt type spherocobaltite lattice, in which Co^{2+}-occupied octahedral sites had little effect on the structure, the Zn^{2+} ions presumably occupy the empty tetrahedral sites in the structure.

Decomposition of the precursors at 350 °C resulted in the loss of CO_2 and water to form ZnO which might have contained some cobalt and/or a zinc-containing Co_3O_4 phase. Generally, monophasic precursors formed monophasic oxides and biphasic precursors formed ZnO and zinc-containing Co_3O_4. No change in lattice parameters was observed for ZnO in the mixed oxides, but systematic shifts were observed for zinc-containing Co_3O_4 which were characteristic of a positive deviation from Vegard's law,[39] indicating that zinc was retained in solid solution in Co_3O_4 originating from the decomposition of either spherocobaltite or basic cobalt carbonate. The formation of monophasic hydrozincite in which Co^{2+} was identified by UV–VIS–NIR diffuse reflectance spectroscopy in Co/Zn 10/90, and decomposition of this to ZnO is evidence, however, that cobalt is present at least in this mixed oxide. For Co/Zn 20/80cal and 30/70cal most of the cobalt was present at the surface as Co^{3+} in the spinel $ZnCo_2O_4$, whereas Co^{2+} was also observed at higher loadings indicating the presence of zinc-containing Co_3O_4 in addition to the surface spinel. It is likely that higher calcination temperatures would be required to extend the spinel into the bulk. This is further substantiated from calculations of the ionic charge from the XPS data. The low cationic charge of the Co^{3+} ions observed for the low cobalt loadings was due to 'surface spinel', $ZnCo_2O_4$, in the vicinity of major quantities of ZnO. As the cobalt was located on the surface, the Co^{3+} ions were located in positions which lowered the overall electronic charge. The surface and near-surface regions became richer in cobalt as the cobalt loading was increased, and hence the surface coverage by the surface spinel increased until for Co/Zn 40/60cal the excess cobalt at the surface resulted in the formation of Co_3O_4 in addition to the surface spinel $ZnCo_2O_4$. The electronic structure of the surface remained constant as the cobalt loading was increased further and hence the true cation charges of the Co^{2+} and Co^{3+} ions for each calcined precursor were very similar for Co/Zn ratios $>40/60$.

Coprecipitation from mixed Co/Zn salts and ammonium carbonate thus results in the precipitation of mixed metal carbonates. Hydrozincite is the only phase formed for Co/Zn $<10/90$. Cobalt substitutes for zinc in octahedral positions in the structure, and increases the thermal stability of the hydrozincite lattice. Biphasic precursors are formed for Co/Zn 20/80 to 50/50, with spherocobaltite becoming the predominant phase as the cobalt concentration is increased. No hydrozincite is detected for Co/Zn 70/30 or 90/10, implying that the solubility of zinc in the cobalt phase is greater than that of cobalt in the zinc phase. On the basis of the anion-exchange hypothesis, the partially anion-exchanged basic cobalt carbonate is formed for Co/Zn 100/0 but is present as a minor phase for Co/Zn 90/10 since $Zn(OH)_2$ is required to catalyse the rapid formation of $Co(OH)_2$ which is subsequently exchanged to form the carbonate. The cobalt-containing hydrozincite phase forms ZnO-containing cobalt in solid solution and the mixed metal precursors with a spherocobaltite structure form zinc-containing Co_3O_4 on calcination. The biphasic precursors decompose to ZnO and Co_3O_4 which probably contain dissolved cobalt and zinc respectively. Most of the cobalt at the surface is present as $ZnCo_2O_4$ for Co/Zn $\leqslant 30/70$; Co_3O_4 is also detected at higher cobalt concentrations. The oxide with the highest surface area is obtained by decomposition of the basic cobalt carbonate precursor.

We are grateful to the EPSRC and ICI Katalco for supporting this work.

References

1 P. J. H. Carnell and P. E. Starkey, *Chem. Eng*., 1984, **408**, 30.
2 T. Baird, P. J. Denny, R. Hoyle, F. McMonagle, D. Stirling and J. Tweedy, *J. Chem. Soc., Faraday Trans*., 1992, **88**, 3375.
3 T. Baird, K. C. Campbell, P. J. Holliman, R. Hoyle, D. Stirling and B. P. Williams, *J. Chem. Soc., Faraday Trans*., 1995, **91**, 3219.
4 T. Baird, K. C. Campbell, P. J. Holliman, R. Hoyle, D. Stirling and B. P. Williams, in *Recent Advances in Oilfield Chemistry*, ed P. H. Ogden, Royal Society of Chemistry, Cambridge, 1994, p. 234.
5 F. Cavani, F. Trifiro and A. Vaccari, *Catal. Today*, 1991, **11**, 173.
6 P. Porta, R. Dragone, G. Fierro, M. Inversi, M. L. Jacono and G. Moretti, *J. Mater. Chem*., 1991, **1**, 531.
7 A. G. Walton, *Chemical Analysis Monograph, Vol. 23, The Formation and Properties of Precipitates*, Wiley-Interscience, London, 1967.
8 P. Porta, S. De Rossi, G. Ferraris, M. Lo Jacono, G. Minelli and G. Moretti, *J. Catal*., 1988, **109**, 367.
9 P. Porta, R. Dragone, G. Fierro, M. Inversi, M. L. Jacono and G. Moretti, *J. Chem. Soc., Faraday Trans*., 1992, **88**, 311.

10 K. Petrov, L. Markov, R. Ioncheva and P. Rachev, *J. Mater. Sci.*, 1988, **23**, 181.
11 D. G. Klissurski and E. L. Uzanova, *J. Mater. Sci. Lett.*, 1990, **9**, 576.
12 D. Briggs and M. P. Seah, *Practical Surface Analysis by Auger and XPS*, Wiley, Chichester, 1985.
13 J. Szajman, J. Liesegang, J. G. Jenkin and R. C. G. Leckey, *J. Electron Spectrosc. Relat. Phenom.*, 1981, **23**, 97.
14 J. H. Schofield, *J. Electron Spectrosc. Relat. Phenom.*, 1976, **8**, 129.
15 N. G. Farr and H. J. Griess, *J. Electron Spectrosc. Relat. Phenom.*, 1989, **49**, 293.
16 JCPDS file no. 19-1458: hydrozincite, $Zn_5(CO_3)_2(OH)_6$.
17 JCPDS file no. 11-692: spherocobaltite, $CoCO_3$.
18 A. M. Khahil and S. Kolboe, *Surf. Technol.*, 1983, **18**, 249.
19 O. Garcia-Martinez, P. Millan, R. M. Rojas and M. J. Torralio, *J. Mater. Sci.*, 1988, **23**, 1334.
20 P. Pappalardo, D. C. Wood and R. C. Linavesta Jr., *J. Chem. Phys.*, 1961, **35**, 2041.
21 J. A. Gadsden, *Infrared Spectra of Minerals and Related Inorganic Compounds*, Butterworths, London, 1975.
22 D. C. Frost, A. McDowell and A. Ishitani, *Mol. Phys.*, 1972, **24**, 861.
23 R. B. Moyes and M. W. Roberts, *J. Catal.*, 1977, **49**, 216.
24 J. S. Hammond, S. W. Gaarenstroom and N. Winograd, *Anal. Chem.*, 1975, **47**, 2194.
25 G. Fierro, R. Dragone, G. Moretti and P. Porta, *Surf. Interf. Anal.*, 1992, **19**, 565.
26 JCPDS file no. 5-664: zinc oxide, ZnO.
27 JCPDS file no. 9-418: cobalt oxide, Co_3O_4.
28 JCPDS file no. 23-1390: zinc cobalt oxide, $ZnCo_2O_4$.
29 A. P. Hagan, C. A. Otero, F. S. Stone and M. A. Trevethan, *Preparation of Catalysts*, vol. 2, ed. B. Delmon, P. Grange, P. Jacobs and G. Poncelet, Elsevier, Amsterdam, 1979.
30 D. S. McClure, *J. Chem. Phys.*, 1962, **36**, 2757.
31 J. Ferraro, *Low Frequency Vibrations of Inorganic and Coordination Compounds*, Plenum Press, New York, 1971.
32 J. J. Chuang, C. R. Brundle and D. W. Rice, *Surf. Sci.*, 1976, **59**, 413.
33 K. Seigbhan, C. Nordling, A. Fahlman, R. Nordberg, K. Harnrin, J. Hedman, G. Johannson, T. Bergmark, S. E. Karlsson, I. Lundgren and B. Lindberg, *ESCA: Atomic, Molecular and Solid State Structure Studied by means of Electron Spectroscopy*, Nova Acta Regiae Sci., Upsalieusis, ser. IV, Almqvist and Wiksells, Uppsala, 1967.
34 J. Q. Broughton and P. S. Bagus, *J. Electron Spectrosc. Relat. Phenom.*, 1980, **20**, 127.
35 T. Dickenson, A. F. Povey and P. M. A. Sherwood, *J. Chem. Soc., Faraday Trans. 1*, 1976, **72**, 686.
36 J. G. Stark and H. G. Wallace, *Chemistry Data Book*, John Murray, London, 1976.
37 J. T. Richardson, *Principles of Catalyst Development*, Plenum Press, New York, 1989.
38 S. Ghose, *Acta Crystallogr.*, 1964, **17**, 1051.
39 A. R. West, *Solid State Chemistry and its Applications*, Wiley, Chichester, 1989.

Paper 6/06759J; *Received* 2*nd October*, 1996